Journal of Power Sources 265 (2014) 1–5

Contents lists available at ScienceDirect

Journal of Power Sources

journal homepage: www.elsevier.com/locate/jpowsour

Short communication

A novel solvent-free thermal reaction of ferrocene and sulfur for one-step synthesis of iron sulfide and carbon nanocomposites and their electrochemical performance

Ling Fei, Yufeng Jiang, Yun Xu, Gen Chen, Yuling Li, Xun Xu, Shuguang Deng, Hongmei Luo*

Department of Chemical and Materials Engineering, New Mexico State University, NM 88003, USA

HIGHLIGHTS

- Iron sulfide was embedded in carbon by thermally reacting ferrocene and sulfur.
- The nanocomposite has iron sulfide nanoparticles sandwiched between carbons.
- The nanocomposite shows excellent electrochemical performance.

ARTICLE INFO

Article history:
Received 28 February 2014
Received in revised form
20 April 2014
Accepted 22 April 2014
Available online 1 May 2014

Keywords:
Ferrocene
Solvent-free
Iron sulfide
Carbon
Lithium ion batteries

ABSTRACT

A novel solvent-free thermal reaction of ferrocene and sulfur is developed for preparing iron sulfide and carbon nanocomposites, where ferrocene acts as both iron and carbon source. The prepared composite has iron sulfide sandwiched in carbon matrix. Moreover, ferrocene and sulfur can turn to vapor phase at an elevated temperature, resulting in easy deposition of product on the surface of templates. Sodium chloride was selected as a template due to its nontoxic and water-soluble nature. The NaCl-templated composite shows “sphere on mattress” morphology and exhibits the highest capacity and the longest cyclability ever reported for iron pyrite anode. To obtain mesoporous nanocomposites, SBA-15 was also applied as templates. The mesoporous nanocomposite demonstrates excellent capacity retention capability, indicating the robust structural stability.

1. Introduction

In recent years, iron pyrite has received significant research attention owing to its earth abundance, nontoxicity, and outstanding performance in a variety of applications [1–4]. For example, its large optical absorption coefficient (6×10^5 cm^{-1}) and high theoretical photovoltaic conversion efficiency (28%) make it an ideal photovoltaic material and photocatalyst [2,5–8]; when considered as electrode material in lithium-ion batteries (LIB), it has high theoretic capacity, and the Li/FeS_2 system possesses advantages of overcharge protection and high temperature operation stability [9–14]. However, if iron sulfide alone is applied as an anode, it usually shows a fast fading capacity and poor rate capability due to its poor electrical conductivity and notorious structural pulverization caused by mechanical strain during the insertion and extraction of lithium ions. Additionally, the formation of polysulfides in the lithium ion storage process worsens the situation. The polysulfides usually exist as insulating layers outside the electrode, which not only further decrease the conductivity and retard the electrochemical reaction process, but also are soluble in organic electrolyte and can gradually migrate to the cathode side, resulting in poor performance and short life of the battery [15–17]. To address above problems, carbon coating is considered to be one of the most effective strategies [16,17]. The carbon plays a crucial role in enhancing the electrochemical performance of materials, e.g. increasing the electrode conductivity thus promotes fast electron transports, maintaining structural integrity under large volume changes during the charging and discharging cycles, and preventing aggregation of nanoparticles. In the case of metal sulphides, carbon coating can reduce or avoid the dissolution of polysulfides by absorbing and trapping them inside [16–18].

* Corresponding author. Tel.: +1 575 646 4204; fax: +1 575 646 7706.
E-mail addresses: hluo@nmsu.edu, luohongmeitulane@yahoo.com (H. Luo).

http://dx.doi.org/10.1016/j.jpowsour.2014.04.110
0378-7753/

To date, there have been a large amount of carbon-based composites as anode materials showing largely enhanced performance [17,19–21]. However, few reports have been dedicated to FeS_2 and carbon composite [9,12]. In those available reports, carbon is usually introduced in three ways: (a) adding pre-carbon precursor like glucose, sugar in the synthetic process of FeS_2 [9]; (b) introducing ready-made carbon materials (e.g. carbon nanotubes, graphene) to the synthetic process [12]; (c) preparing FeS_2 first then coated it with carbon or polymers [22]. In the first case, post-annealing steps are often required, while carbon materials are supplied in the second case, and the third one is a multiple-step process. Moreover, in many reports, the preparation of FeS_2 via solvothermal synthesis requires hazardous organic solvents or surfactants (e.g. oleylamine, oleic acid) [23,24].

Herein, we report a single-step solvent-free thermal reaction of ferrocene and sulfur for preparing FeS_2@C. Under this scenario, ferrocene, a sandwich compound with a central Fe atom bounded to two cyclopentadienyl rings, is used as both iron and carbon source. Because ferrocene and sulfur can turn to vapor phase at an elevated temperature, they can be easily deposited on the surface of various templates. Here, we prepared water-soluble NaCl templated FeS_2@C nanocomposites. When applied as electrode materials in LIB, the NaCl-templated composite exhibits the best electrochemical performance: maintaining a discharge capacity of 681.8 mAh g^{-1} even after 100 cycles at a current density of 100 mA g^{-1}, which is the highest capacity with the longest cyclability reported for FeS_2. Additionally, when SBA-15 is applied as template, mesoporous FeS@C nanocomposite can be obtained.

2. Material and methods

In a typical experimental procedure, 0.93 g ferrocene (Aldrich, 98%) and 0.4 g sulfur (Aldrich, 99.98%) were well mixed and ground with a pestle and mortar then wrapped by alumina foil. The mixture was annealed at 500 °C for 2 h in flowing N_2 atmosphere to obtain the final FeS_2@C product. Templated products were prepared in the same procedure, except that 5 g NaCl (Aldrich, 99.5%, particle size 0.5–0.7 mm) or 0.4 g SBA-15 (detailed synthetic procedure, porosity, morphology can be found in our previous work [25]) were introduced to ferrocene and sulfur before mixing and grinding. After the reaction, NaCl was washed away by deionized water while SBA-15 was removed by NaOH. The schematic synthetic procedure for the synthesis of FeS_2@C nanocomposites is shown in Fig. 1(a). For simplicity, the sample prepared without templates is noted as FeS_2@C, and the NaCl templated sample named as NaCl–FeS_2@C (NaCl has been washed away). Because the product templated by SBA-15 exhibits different crystalline phase from the FeS_2@C and NaCl–FeS_2@C, it will be discussed separately.

The structure and morphology of the samples were characterized by X-ray diffraction (XRD, Cu Kα) and transmission electron microscopy (TEM, JEOL-2010, 200 kV). The Brunauer–Emmett–Teller (BET) specific surface area of the sample was determined by an ASAP 2020 using the standard N_2 adsorption and desorption isotherm measurements at 77 K. Electrochemical measurements were conducted using CR-2032 coin cells. The working electrode was prepared by casting slurry (70 wt% of active materials, 20 wt% of carbon black, and 10 wt% of polyvinylidene fluoride binder in N-methyl-2-pyrrolidinone) onto the nickel foam (MTI, Purity > 99.99%, 1.6 mm), and dried in a vacuum oven at 70 °C for 12 h to remove the solvent. Electrode material thickness is around 10 μm and has a density of 2 mg cm^{-2}. A lithium foil was used as the counter electrode and a mixture of 1 M $LiPF_6$ in ethylene carbonate (EC)/dimethyl carbonate (DMC) (1:1 in volume) was used as the electrolyte. Cell assembly was carried out in an argon-filled glove-box with an oxygen concentration below 1 ppm. The galvanostatic charge/discharge measurements were performed using a Land battery testing system in the cutoff voltage window of 0.005–3 V (vs. Li^+/Li).

3. Results and discussion

A chemical reaction is proposed in Fig. 1(b) to represent the formation of iron sulfide and carbonization of cyclopentadienyl rings in the annealing process. The XRD patterns of FeS_2@C and NaCl–FeS_2@C are shown in Fig. 1(c). The diffraction peaks of both nanocomposites can be attributed to FeS_2 (JCPDS 65-3321). The peaks are not very sharp, indicating the low crystallinity of the nanocomposites. Fig. 2(a)–(c) shows the TEM images of FeS_2@C nanocomposite prepared without template. As can be seen in Fig. 2(a), the composite mainly contains large aggregates. Higher magnification images (Fig. 2(b) and (c)) reveal that the microstructure of FeS_2@C has FeS_2 nanoparticles sandwiched within carbon (carbon/FeS_2/carbon), which may be inherited from the sandwich molecular structure of ferrocene (cyclopentadienyl ring/Fe/cyclopentadienyl ring). When NaCl was added into the synthetic procedure, the product (NaCl–FeS_2@C), as shown in Fig. 2(d), has many spheres with diameter around 750 nm sitting on a "composite mattress". The flat bare mattress and a small part of composite falling off from spheres are exhibited in Fig. 2(e) and (f), respectively. Both have the same microstructure as that FeS_2 nanoparticles are embedded in carbon matrix. A possible formation mechanism of the "sphere on mattress" structure is proposed: in the annealing step, ferrocene and sulfur were first deposited on the surface of sodium chloride particles to form the flat "mattress". The already formed nanoparticles on the surface of "mattress" can act as nucleation sites for further formation and growth of spheres.

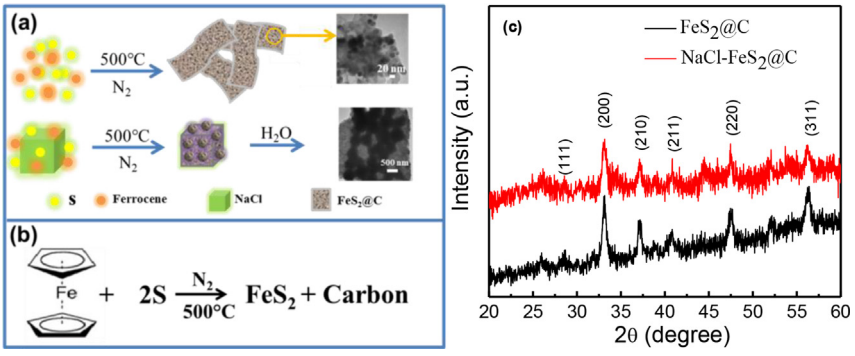

Fig. 1. (a) Schematic illustration of the synthetic procedure of FeS_2@C composites; (b) the proposed chemical reaction for the synthetic procedure; (c) XRD patterns of FeS_2@C and NaCl–FeS_2@C composites.

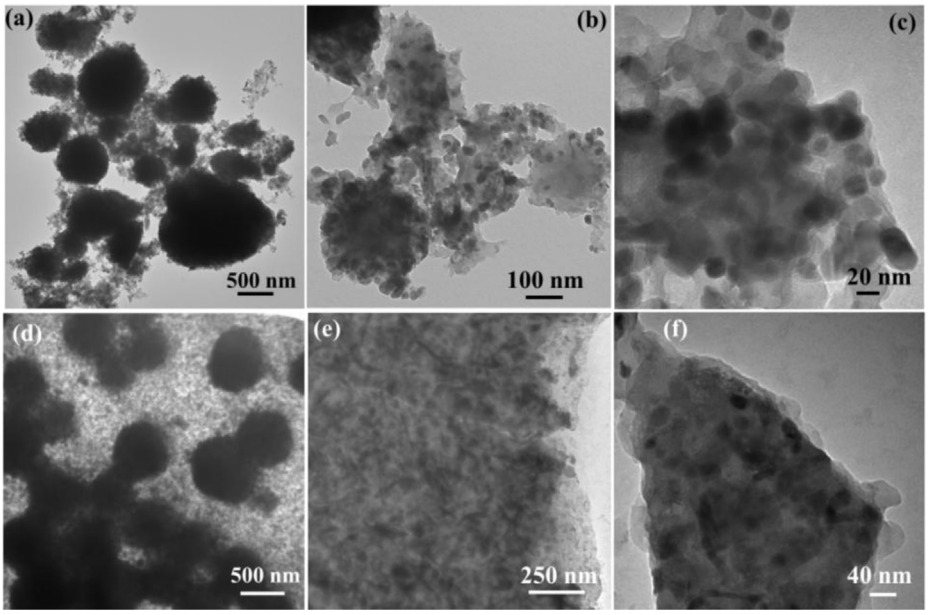

Fig. 2. TEM images of (a–c) FeS_2@C composite; (d–f) NaCl–FeS_2@C composite.

It is believed that carbon-based composites are promising for lithium ion batteries. Thus, FeS_2@C and NaCl–FeS_2@C were assembled into half-cells and evaluated by galvanic charge and discharge in a voltage range of 0.005–3 V (vs. Li^+/Li). Fig. 3(a) displays the discharge/charge voltage profile of the NaCl–FeS_2@C for the first, second, third, and 100th cycles at a current density of 100 mA g^{-1}. The initial discharge plateaus around 1.2 V is attributed to the lithiation reaction of FeS_2 to form Li_2S and Fe, while the two charge plateaus around 1.9 and 2.2 V correspond to the formation of $Li_{2-x}FeS_2$, Li and further transformation to FeS_y, S, and Li [9–11]. In addition, the initial discharge capacity for NaCl–FeS_2@C sample is 1446.7 mAh g^{-1}, with the corresponding charge capacity of 1024.6 mAh g^{-1}, giving the initial Coulombic efficiency of 70.8%. The low initial Coulombic efficiency is caused by the irreversible consumption of lithium ions due to the formation of the solid electrolyte interphase (SEI) layers. The cyclic performance of the

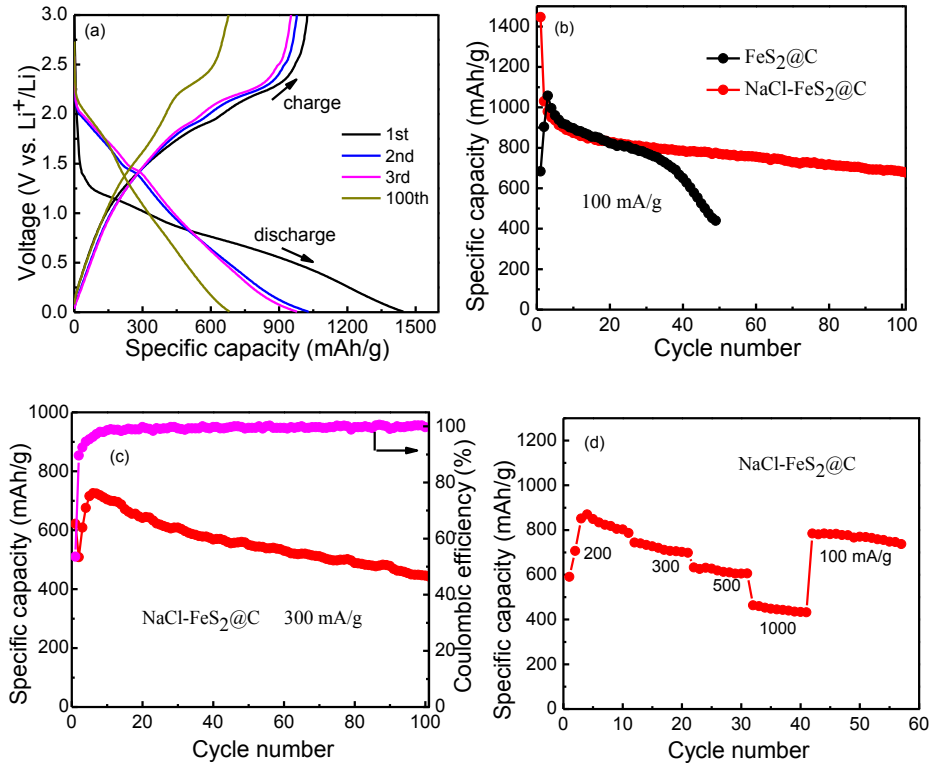

Fig. 3. (a) Voltage profile of NaCl–FeS_2@C at a current density of 100 mA g^{-1}; (b) cycle performance of the two nanocomposites at 100 mA g^{-1}; (c) cycle performance of NaCl–FeS_2@C nanocomposite at 300 mA g^{-1}; (d) rate performance of NaCl–FeS_2@C nanocomposite.

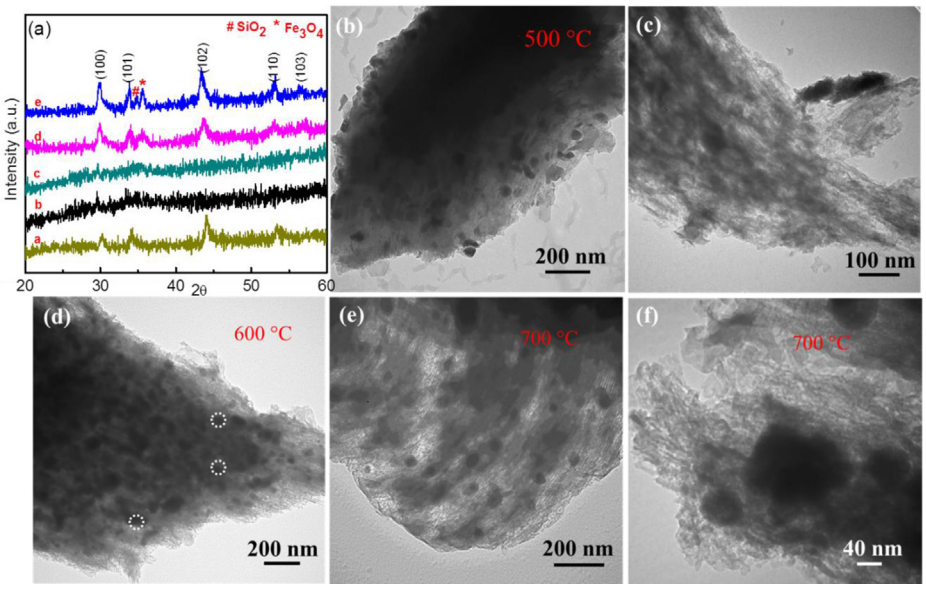

Fig. 4. (a) XRD patterns of SBA-15 templated composites (a. the composite obtained within SBA-15; b. the composite after the removal of SBA-15; the template-free composite further annealed at c. 500 °C for 1 h, d. 600 °C for 1 h, e. 700 °C for 1 h); TEM images of (b) the composite within SBA-15; (c) the composite after removal of SAB-15; the obtained template-free sample annealed at (d) 600 °C, and (e,f) 700 °C for 1 h.

two samples at a current density of 100 mA g^{-1} is presented in Fig. 3(b). As can be seen, FeS_2@C and NaCl–FeS_2@C show similar capacities in the first 25 cycles, except the discharge capacities of the first and the second cycles of FeS_2@C are lower that that of the third cycle. This phenomenon may be induced by the larger aggregates (Fig. 2(a)) of FeS_2@C sample, where the longer ion diffusion and electron transfer path result in retarded electrochemical reaction. After 30 cycles, FeS_2@C suffers fast fading capacity, while NaCl–FeS_2@C nanocomposite demonstrates a stable and robust cyclic performance. After 100 cycles, the NaCl–FeS_2@C nanocomposite still remains a reversible discharge capacity of 681.8 mAh g^{-1}, the highest capacity and longest cyclability reported to date for FeS_2 based materials: 420 mAh g^{-1} of FeS_2 nanoparticles after 30 cycles at 0.1C (1C = 890 mA g^{-1}) [10]; 495 mAh g^{-1} of FeS_2/C after 50 cycles at a very low current density of 0.05C [9]; 427 mAh g^{-1} of FeS_2 nanocrystals at 0.1 C after 40 cycles [3]; and 491 mAh g^{-1} of FeS_2/CNT at 0.1 C after 50 cycles [12]. Moreover, the NaCl–FeS_2@C delivers a high capacity of 445.7 mAh g^{-1} even after being cycled at a higher current density of 300 mA g^{-1} for 100 cycles (Fig. 3(c)). The overall Coulombic efficiency among the 100 cycles is above 99%.

Fig. 3(d) displays the rate performance of the NaCl–FeS_2@C composite at different current densities. As expected, its specific capacity decreases with the increase of the current densities: the electrode delivered a capacity of ~820 mAh g^{-1} at 200 mA g^{-1}, ~720 mAh g^{-1} at 300 mA g^{-1}, ~615 mAh g^{-1} at 500 mA g^{-1}, and ~440 mA g^{-1} at 1000 mA g^{-1}, respectively. When the current density was changed to 100 mA g^{-1}, the specific capacity rebounded to ~760 mAh g^{-1}, showing very small capacity loss. The excellent electrochemical performance of NaCl–FeS_2@C could be attributed to the robust "sphere on mattress" architecture and the microstructure of FeS_2 sandwiched between carbon. The carbon matrix not only increases the electrode conductivity, but also acts as a buffer layer that maintains structural integrity of the electrode despite large volume changes during the charging and discharging cycles, as well as hinders aggregation of FeS_2 particles. Compared with those nanostructures having nanoparticles anchored on the surface of carbon layers, the sandwiched nanostructure also has the advantage of preventing particles falling off during cycling process. Additionally, the FeS_2 itself acts as spacer to allow easy penetration of electrolyte and fast diffusion of Li ions. More importantly, the carbon matrix can reduce or avoid the dissolution of polysulfide by absorbing and trapping it inside.

In order to obtain mesoporous iron sulfide and carbon nanocomposite, SBA-15 was also applied as template. Interestingly, the SBA-15 templated product is FeS (JCPDS #65-9124) rather than FeS_2 phase, as confirmed by XRD patterns (Fig 4(a),a). We also found that the SBA-15 removal treatment by NaOH has influence on FeS nanoparticles. The XRD patterns in Fig. 4(a) and (b) show that the composite become amorphous after the NaOH treatment, which may indicate the decomposition of FeS. The amorphous composite can be recrystallized to FeS at an annealing temperature above 600 °C, as determined in Fig. 4(a), (d) and (e). Two additional small peaks from SiO_2 residue and Fe_3O_4 were observed. The Fe_3O_4 is probably generated from the oxidation of metastable FeS. The XRD analysis is consistent with the TEM images. As can be seen in Fig 4(b), the composite before removing template contains some FeS nanoparticles. However, after the removal treatment of SBA-15, the FeS nanoparticles disappear, leaving amorphous phase behind (Fig. 4(c)), which explains why no peak is found in the XRD pattern. Fig. 4(d), (e) and (f) shows the images of template-free composite annealed at 600 or 700 °C. It can be seen that the FeS nanoparticles were regrown in the mesoporous carbon matrix. N_2 adsorption/desorption measurement was conducted to study the specific surface area and porosity of FeS@C (annealed at 700 °C). As can be seen from Fig. 5(a), the N_2 adsorption/desorption isotherm profile of FeS@C has the typical characteristics of mesoporous materials, type IV curve. The FeS@C has a very large BET surface area of 440.3 m^2 g^{-1} with pore size around 4 nm.

It is interesting that SBA-15 results in the formation of FeS rather than FeS_2. After carefully reviewing and comparing the reaction process, we realized that the actual amount of sulfur, which can be readily accessed by ferrocene vapor, should be responsible for the formation of different products. In the experiments, ferrocene and sulfur with or without templates were mixed together first, then turned to vapor phase for the synthetic reaction of iron sulfides. When there is no template or solid NaCl is applied, the sulfur vapor is always adequate for the given amount of ferrocene to form FeS_2,

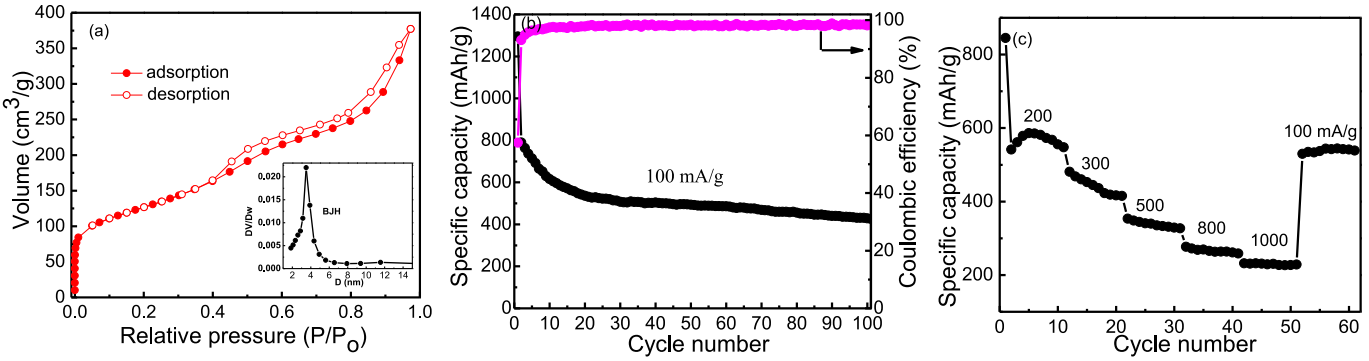

Fig. 5. (a) N_2 adsorption/desorption isotherm of FeS@C (annealed at 700 °C) at 77 K; (b) Cycle performance of FeS@C (700 °C) nanocomposite at a current density of 100 mA g^{-1}; (c) rate performance of FeS@C (700 °C) nanocomposite.

because sulfur is over supplied in the experimental process. However, in the case of SBA-15, the reaction of ferrocene and sulfur are taken place in the mesochannels (~11 nm) of SBA-15. Before iron sulfide can be formed, ferrocene and sulfur both need to diffuse into the small channels. In other words, they have to compete with each other to enter the space-limited reaction site. Under this scenario, although sulfur is over supplied, it is not enough for the formation of FeS_2 in the space-limited mesochannels, therefore, FeS is formed. To make it simple, in the case of SBA-15, sulfur is the limited reactants, while ferrocene is the limited one in the case of no template or solid NaCl template synthesis.

We also studied the electrochemical performance of the SBA-15 templated mesoporous FeS@C sample. The cyclic performance is shown in Fig. 5(b). As observed, it delivers a high initial discharge capacity of 1294.8 mA g^{-1} and remains a second discharge cycle capacity of 789.6 mA g^{-1}. The discharge capacity shows a clear decrease in the first 20 cycles. Afterward, the cyclic performance is much more stable and demonstrates a capacity of 428.57 mA g^{-1} even after 100 cycles. Over the 100 cycles, the Coulombic efficiency remains around 98%. When cycled at different current densities, the FeS@C also shows good rate capabilities (Fig. 5(c)). As the current density increases from 200 mA g^{-1} to 300 mA g^{-1}, 500 mA g^{-1}, 800 mA g^{-1}, and 1000 mA g^{-1}, the specific capacities change from ~570 mAh g^{-1} to 440 mAh g^{-1}, 340 mAh g^{-1}, 260 mAh g^{-1}, and 220 mAh g^{-1}, respectively. Once the current density was changed to 100 mA g^{-1}, the specific capacity rebounded to ~540 mAh g^{-1}, demonstrating good capacity retention. Note that the FeS@C sample has lower capacity value in comparison to NaCl–FeS_2@C, which could be due to the lower theoretical capacity of FeS and its partial loss in the SiO_2 removal step. Considering the requirements of strong base or hydrofluoric acid for SiO_2 removal and the accompanied FeS loss, the NaCl templated FeS_2@C is the better choice for batteries materials. While the mesoporous nature of FeS@C may make it a good candidate for catalyst application.

4. Conclusion

In summary, a solvent-free thermal reaction of ferrocene and sulfur has been developed for preparing iron sulfide and carbon nanocomposites, where ferrocene acts as both carbon and iron source. Because both ferrocene and sulfur turn to vapor phase at an elevated temperature, the final product can be easily deposited on the surface of templates with controllable morphology. Due to the advantageous microstructure of iron sulfide nanoparticles sandwiched in carbon matrix, the composites show excellent electrochemical performance. Especially, the NaCl template N–FeS_2@C maintains a capacity of 681.8 mAh g^{-1} at 100 mA g^{-1} after 100 cycles, higher than all the reported values for iron pyrite anode.

Acknowledgment

We acknowledge the funding support from NSF/CMMI Nano-Manufacturing Program under Grant No. 1131290 and the office of Vice President for Research at NMSU. X. X. acknowledges the GREG award and L. F. acknowledges the Preparing Future Faculty Graduate Assistantship Award.

References

[1] X. Chen, Z. Wang, X. Wang, J. Wan, J. Liu, Y. Qian, Inorg. Chem. 44 (2005) 951–954.
[2] Y. Bai, J. Yeom, M. Yang, S.-H. Cha, K. Sun, N.A. Kotov, J. Phys. Chem. C. 117 (2013) 2567–2573.
[3] F.M. Hassan, V. Chabot, A.R. Elsayed, X. Xiao, Z. Chen, Nano Lett. 14 (2014) 277–283.
[4] D.-W. Wang, Q.-H. Wang, T.-M. Wang, CrystEngComm. 12 (2010) 755–761.
[5] M. Caban-Acevedo, M.S. Faber, Y. Tan, R.J. Hamers, S. Jin, Nano. Lett. 12 (2012) 1977–1982.
[6] M. Gong, A. Kirkeminde, N. Kumar, H. Zhao, S. Ren, Chem. Commun. 49 (2013) 9260–9262.
[7] Q.-H. Huang, T. Ling, S.-Z. Qiao, X.-W. Du, J. Mater. Chem. A 1 (2013) 11828–11833.
[8] R. Morrish, R. Silverstein, C.A. Wolden, J. Am. Chem. Soc. 134 (2012) 17854–17857.
[9] D. Zhang, Y.J. Mai, J.Y. Xiang, X.H. Xia, Y.Q. Qiao, J.P. Tu, J. Power Sources 217 (2012) 229–235.
[10] D. Zhang, J.P. Tu, J.Y. Xiang, Y.Q. Qiao, X.H. Xia, X.L. Wang, C.D. Gu, Electrochim. Acta 56 (2011) 9980–9985.
[11] R. Fong, J.R. Dahn, C.H.W. Jones, J. Electrochem. Soc. 136 (1989) 3206–3210.
[12] L. Liu, Z. Yuan, C. Qiu, J. Liu, Solid State Ionics 241 (2013) 25–29.
[13] Yang Shao-Horn, Q.C. Horn, Electrochim. Acta 46 (2001) 2613–2621.
[14] X. Li, P. Meduri, X. Chen, W. Qi, M.H. Engelhard, W. Xu, F. Ding, J. Xiao, W. Wang, C. Wang, J.-G. Zhang, J. Liu, J. Mater. Chem. 22 (2012) 11014.
[15] B. Wu, H. Song, J. Zhou, X. Chen, Chem. Commun. 47 (2011) 8653–8655.
[16] L. Fei, Q. Lin, B. Yuan, G. Chen, P. Xie, Y. Li, Y. Xu, S. Deng, S. Smirnov, H. Luo, ACS Appl. Mater. Interf. 5 (2013) 5330–5335.
[17] C. Xu, Y. Zeng, X. Rui, N. Xiao, J. Zhu, W. Zhang, J. Chen, W. Liu, H. Tan, H.H. Hng, Q. Yan, ACS Nano 6 (2012) 4713–4721.
[18] X. Ji, K.T. Lee, L.F. Nazar, Nat. Mater. 8 (2009) 500–506.
[19] Y. Gu, Y. Xu, Y. Wang, ACS Appl. Mater. Interf. 5 (2013) 801–806.
[20] L. Fei, Q. Lin, B. Yuan, M. Naeemi, Y. Xu, Y. Li, S. Deng, H. Luo, Mater. Lett. 98 (2013) 59–62.
[21] C. Zhang, Z. Wang, Z. Guo, X.W. Lou, ACS Appl. Mater. Interf. 4 (2012) 3765–3768.
[22] D. Zhang, J.P. Tu, J. Zhang, Y.Q. Qiao, X.L. Wang, J. Aust. Ceram. Soc. 48 (2012) 189–193.
[23] A. Kirkeminde, B.A. Ruzicka, R. Wang, S. Puna, H. Zhao, S. Ren, ACS Appl. Mater. Interf. 4 (2012) 1174–1177.
[24] B. Yuan, W. Luan, S.T. Tu, Dalt. Trans. 41 (2012) 772–776.
[25] L. Fei, Y. Xu, X.F. Wu, Y.L. Li, P. Xie, S.G. Deng, S. Smirnov, H.M. Luo, Nanoscale 5 (2013) 11102–11107.